PNAS RESEARCH ARTICLE | DEVELOPMENTAL BIOLOGY
BIOPHYSICS AND COMPUTATIONAL BIOLOGY OPEN ACCESS

Formation of recurring transient Ca^{2+}-based intercellular communities during *Drosophila* hematopoiesis

Saar Ben David[a,1], Kevin Y. L. Ho[b,1], Guy Tanentzapf[b,2], and Assaf Zaritsky[a,2]

Edited by K. VijayRaghavan, Tata Institute of Fundamental Research, Bangalore, India; received October 23, 2023; accepted March 8, 2024

Tissue development occurs through a complex interplay between many individual cells. Yet, the fundamental question of how collective tissue behavior emerges from heterogeneous and noisy information processing and transfer at the single-cell level remains unknown. Here, we reveal that tissue scale signaling regulation can arise from local gap-junction mediated cell–cell signaling through the spatiotemporal establishment of an intermediate-scale of transient multicellular communication communities over the course of tissue development. We demonstrated this intermediate scale of emergent signaling using Ca^{2+} signaling in the intact, ex vivo cultured, live developing *Drosophila* hematopoietic organ, the lymph gland. Recurrent activation of these transient signaling communities defined self-organized signaling "hotspots" that gradually formed over the course of larva development. These hotspots receive and transmit information to facilitate repetitive interactions with nonhotspot neighbors. Overall, this work bridges the scales between single-cell and emergent group behavior providing key mechanistic insight into how cells establish tissue-scale communication networks.

calcium signaling | *Drosophila* hematopoiesis | multicellular synchronization | cell–cell communication | quantitative live imaging

Significance

Cells coordinate their internal state and behavior by exchanging information with other cells in their vicinity. These local interactions are integrated across space and time to enable tissue scale synchronized function. Using live microscopy imaging of the *Drosophila* lymph gland, and by applying computational analyses, we identified and characterized a mode of cellular communication through self-organized recurring coordinated short-term activation at the intermediate scale of three to eight cells, which we call "hotspots". We reveal that hotspots form over the course of tissue development, and are dependent on specific proteins, called gap-junctions, that enable communication between adjacent cells. Hotspots repeatedly transmit and retrieve information to and from their nonhotspot neighbors to spread information throughout the tissue to regulate and coordinate tissue function.

The emergence of collective cell behavior is an essential component of many basic biological phenomena such as tissue morphogenesis (1), cell migration (2), or bacterial quorum sensing (3, 4). Key to understanding collective cell decision-making is elucidating how local information transfer between cells is integrated in space and time. This spatial and temporal integration of information is essential for regulating the emergence of collective behavior at the multicellular scale (5, 6). The *Drosophila* hematopoietic organ, the lymph gland (LG), is a powerful, genetically tractable, model to study how information is integrated in space and time to facilitate collective cell behavior. The LG contains dozens of blood progenitors that can be collectively activated under certain conditions, such as in response to pathogenic infection, to rapidly produce hundreds of highly differentiated blood cells with infection-fighting characteristics (7, 8). Long-term culture and live imaging of the intact LG showed that Calcium (Ca^{2+}) signaling, which is transmitted between blood progenitor cells through gap-junctions, mediated essential information transfer across large distances in the LG (9). Ca^{2+} levels serve a key function in controlling blood progenitor fate as the activity of multiple pathways that regulate progenitor behavior, including JAK/STAT and CaMKII signaling, is modulated by the amount and activation rate of Ca^{2+} in the cell at a specific time (9, 10). Gap junctions, intracellular channels that directly link adjacent cells to allow them to exchange ions and other small molecules, can help cells form signaling networks (9, 11, 12). The signaling network equilibrates Ca^{2+} signals, that originate from both extracellular and intracellular sources, across blood progenitors, ensures uniform activation of the downstream Ca^{2+} effector CaMKII, and coordinates blood progenitor proliferation and differentiation during hematopoiesis (9). In characterizing, at the population scale, the gap-junctions-based, Ca^{2+}-mediated, multicellular signaling network in the LG we observed synchronized cell pairs that were located up to 190 μm from one another. Importantly, functional studies illustrated that the gap-junction mediated Ca^{2+}-signaling network was required for proper regulation and function of the LG by coordinating fate decisions at the population scale (9). Specifically, blocking the activity of gap junctions perturbed the Ca^{2+} signaling network, altered the quality of encoded information, and led to an abnormally accelerated differentiation and depletion of the blood progenitor population (9). Increasing the level of Ca^{2+} or its downstream signaling activity by knocking down SERCA and/or by overexpression of CaMKII, respectively, restored blood progenitor homeostasis in the absence of gap junction-mediated communication (9). These results suggested that gap junctions maintain hematopoietic homeostasis and guide cell fate decisions by regulating Ca^{2+} signaling.

A key question that emerged from our previous work was how local information transfer between adjacent cell pairs led to the formation of a global multicellular network.

Author affiliations: [a]Department of Software and Information Systems Engineering, Ben-Gurion University of the Negev, Beer-Sheva 84105, Israel; and [b]Department of Cellular and Physiological Sciences, University of British Columbia, Vancouver V6T 1Z3, Canada

Author contributions: G.T. and A.Z. designed research; S.B.D., K.Y.L.H., G.T., and A.Z. performed research; S.B.D. analyzed data; and S.B.D., K.Y.L.H., G.T., and A.Z. wrote the paper.

The authors declare no competing interest.

This article is a PNAS Direct Submission.

[1]S.B.D. and K.Y.L.H. contributed equally to this work.

[2]To whom correspondence may be addressed. Email: guy.tanentzapf@ubc.ca or assafzar@gmail.com.

This article contains supporting information online at https://www.pnas.org/lookup/suppl/doi:10.1073/pnas.2318155121/-/DCSupplemental.

Published April 11, 2024.

Specifically, we wanted to characterize and understand the intermediate stages that allowed cell–cell signaling exchanged between individual cells to become collective signaling. Here we identified, using spatiotemporal analysis of Ca^{2+}-signaling in live intact LGs, the gradual formation of communicating communities of 3 to 14 progenitor cells over the course of development, through intercellular gap junction-mediated signaling. Recurrent signaling activity of these communities formed hotspots of local information transmission highlighting heterogeneity in intercellular information transfer as a potential contributor to collective decision-making. Taken together, our results explain how the exchange of information between individual cells in the *Drosophila* LG becomes an emergent behavior involving multiple cells. This provides insight into the bridging of the scales between single-cell and emergent group behavior.

Results

Propagating Intercellular Ca^{2+} Signaling Forms Communicating Communities in the *Drosophila* LG. We investigated Ca^{2+} signaling in individual blood progenitors using live imaging of intact, ex vivo cultured, LGs (Fig. 1*A*). By manual qualitative selection of adjacent blood progenitor pairs, we previously showed that Ca^{2+} signals propagate between neighboring blood progenitor pairs and this propagation is mediated by gap junctions (Movie S1) (9). To systematically and quantitatively characterize the patterns of signal synchronization across scales in-depth, we measured the temporal correlation between Ca^{2+} signals in all blood progenitor pairs in the LG. This analysis identified a negative correlation between the distance between blood progenitor pairs (termed cell pair distance) and the level of coordination in their Ca^{2+} signals (termed cell pair correlation), that was not sensitive to the local cell density (Fig. 1*B* and *SI Appendix*, Fig. S1*A*). This means that, on average, closer blood progenitor pairs were more synchronized in terms of Ca^{2+} signaling than distant pairs. These data identified a subpopulation of highly synchronized cell pairs, where cells were located within a distance of approximately 14 μm from one another, about two cell diameters apart. Indeed, partitioning the data to close (≤14 μm) versus far (≥14 μm) cell pairs showed that close pairs were more likely to be in a higher level of synchronization (Fig. 1*C* and *SI Appendix*, Fig. S1*B*). This subpopulation of highly synchronized close-cell pairs highlighted the heterogeneity in cell–cell information transfer. However, it was still unclear how this local cell–cell synchronization propagates from the scale of cell pairs to the multicellular scale.

To detect and quantify collective spatiotemporal signaling events, i.e., signaling events that involve more than two cells, we applied a computational method known as the "Automatic Recognition of COllective Signaling" (ARCOS) (13). ARCOS binarizes the single blood progenitor Ca^{2+} signal, according to its magnitude, to "active" (Ca^{2+} peak) or "inactive", followed by spatiotemporal grouping of cells that were synchronously active (peaks ≤ 15 s apart) and within a distance of 14 μm from one another (*SI Appendix*, Fig. S2 *A* and *B*; see *Materials and Methods*) (13). This analysis defined "collective signaling events" that we referred to as local transient communities of blood progenitor signaling (Movie S2). Every community consisted of a minimum of three cells that were active simultaneously or within a 15-s delay. Using ARCOS, we were able to monitor the formation and disintegration of a community (Fig. 1*D* and Movie S3): Following an initial Ca^{2+} spike, subsequent activation of adjacent blood progenitors, as marked by red dots connected by a white arrow, initiated a 3-cell community (Fig. 1*D*, 0 to 7 s). The community gradually grew, which was observed as Ca^{2+} activation in adjacent cells (Fig. 1*D*, red dots and white arrows, 11 to 23 s) and shrunk by deactivation of cells in the community (Fig. 1*D*, yellow arrowheads, 18 to 25 s). Throughout its evolution, this community involved six cells (Fig. 1*D*, marked by a white dashed polygon, 25 s) with a maximum of five cells being active simultaneously (Fig. 1*D*, 16 s). Our analysis identified communities of local intercellular transfer of signaling information involving 3 to 14 blood progenitors per community, with a median community size of four cells and 30% of communities having at least five participating cells (*SI Appendix*, Fig. S2*C*, an example in Movie S3), where cells participating in communities had lower relative Ca^{2+} spike magnitudes than those absent from any community (*SI Appendix*, Fig. S3; see *Materials and Methods*). Two potential confounders of this analysis were the stochastic coincidence of activation events and the presence of areas with higher local cell densities, both of which may lead to the detection of spurious collective signaling events by ARCOS (*SI Appendix*, Fig. S4). To mitigate these potentially confounding factors, we spatially shuffled the cells (i.e., randomized their location), applied ARCOS to identify collective signaling events in the spatially permuted experiment, and recorded the mean number of collective signaling events per cell (mean events per cell, MEC) across the entire population. We repeated the sequence of random shuffling and ARCOS analysis 1,000 times (Fig. 1*E*) and recorded: A) the statistical significance - the fraction of times that the MEC of these in silico spatially permuted experiments were equal or exceeded the MEC of the observed (unpermuted) experiment. Experiments with statistical significance ≤ 0.05 were referred to as "spatially significant" (*Materials and Methods*). B) the magnitude - the ratio between the experimentally observed MEC and the mean MEC of each of its in silico spatial permutations (*Materials and Methods*). All replicates, but one (11/12), were spatially significant, showing elevated magnitude of the MEC, by a factor of 1.2-fold to 3.3-fold in respect to the in silico permuted experiments, indicating that the collective signaling events were a local property of this multicellular system (Fig. 1*F* and *SI Appendix*, Fig. S5). Cell pairs that participated, at least once, in the same transient community ("intracommunity") were more synchronized (i.e., temporally correlated) than cell pairs that participated in different communities ("intercommunity"), i.e., "actively" communicating cells that never interacted directly, confirming enhanced intercellular synchronization in communities (*SI Appendix*, Fig. S6). Altogether, our data suggests that local cell–cell information transfer integrates in space and time to form multicellular communities of Ca^{2+} signal propagating blood progenitors in live intact ex vivo cultured LGs.

Gap Junctions Mediate the Propagation of Ca^{2+} Signals in Blood Progenitor Communities. We previously demonstrated that gap junctions were required for cell-to-cell Ca^{2+} propagation between the blood progenitors in the *Drosophila* LG (9). To assess the role of gap junctions in the formation of intercellular communities, we analyzed ex vivo cultured LGs using live imaging under different conditions where gap junctions were perturbed. Specifically, we used both a genetic and a pharmaceutical-based approach to disrupt gap junction-mediated communication between blood progenitors. First, we used an RNA interference (RNAi) approach to knock down the expression of the gap junction protein Innexin 4, known by its gene name *zero population growth*, or *zpg* (14). We have previously shown that Zpg is the main gap junction channel mediating Ca^{2+} signaling between blood progenitors (9). Second, we used the gap-junction blocker known as carbenoxolone (CBX). We performed RNAi-mediated knockdown of *zpg* (N = 8), a low-dose CBX treatment (3.125 μM; N = 3), a high-dose CBX treatment (12.5 μM, N = 4), or a control where we first

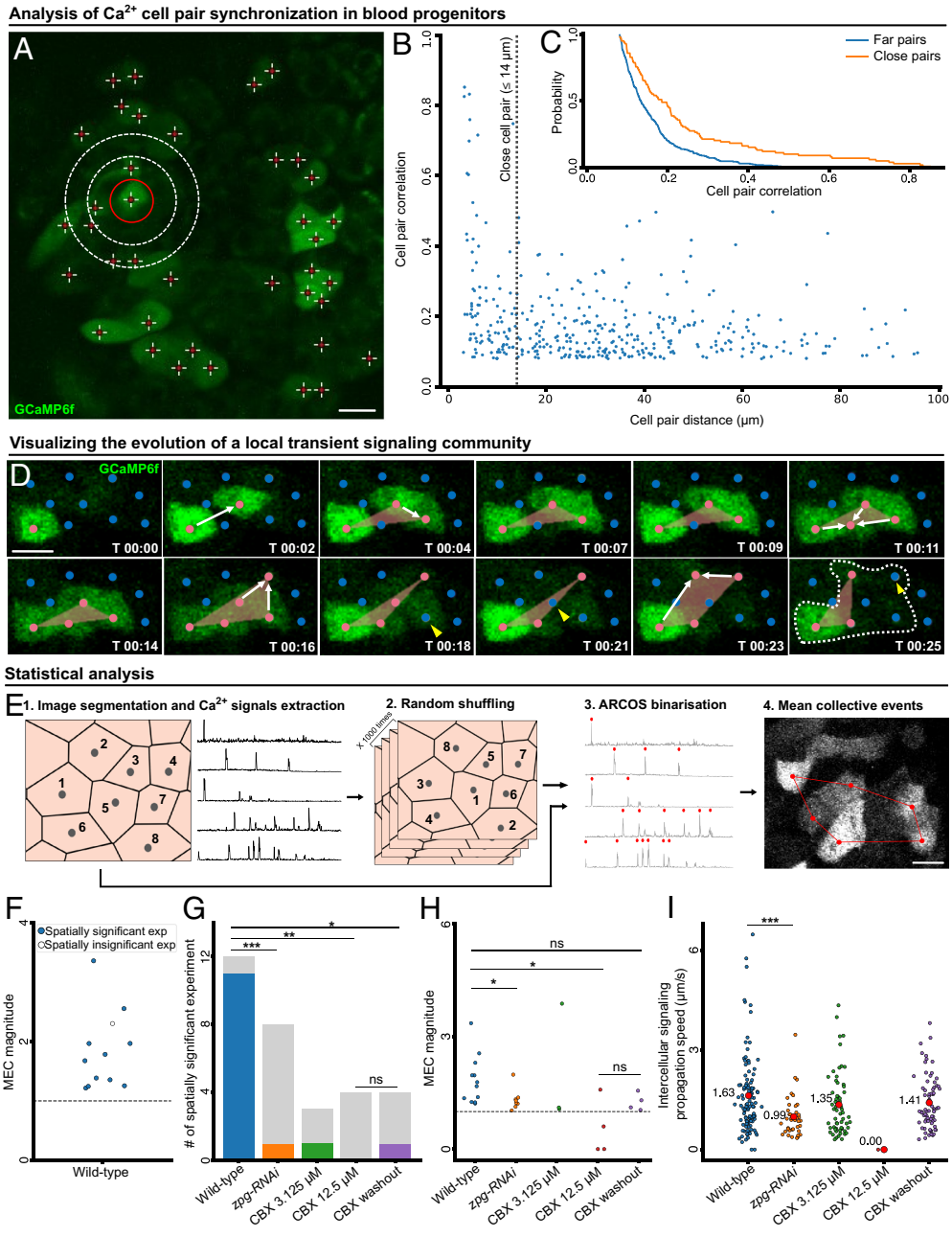

Fig. 1. Blood progenitor cell–cell communication forms communities of propagative Ca^{2+} signaling. (*A*) Representative confocal image showing Ca^{2+} signaling activities in blood progenitors of a LG visualized using GCaMP6f (in green). Red crosses indicate the center of individual cells. White circles indicate adjacent blood progenitors to the cell marked by the red circle, at distances of 7 μm and 14 μm from it correspondingly (Movie S1). (Scale bar: 10 μm.) (*B*) Spatial analysis of blood progenitor pairs that showed a statistically significant correlation ($P < 0.05$) in their temporal Ca^{2+} signals. Each data point (blue) represents a cell pair. Cell pairs Ca^{2+} Pearson correlation was correlated with the cell pairs distance. $N_{cells} = 57$, $N_{pairs} = 385$, Pearson correlation between cell pair Ca^{2+} correlation and distance = −0.244, *P*-value = 0.003. See also *SI Appendix*, Fig. S1*A* for an analysis of all cell pairs. (*C*) Cumulative distribution of Pearson correlation of the close (orange; N = 98, μ = 0.246, σ = 0.187) and far (blue; N = 287, μ = 0.160, σ = 0.084), significantly Ca^{2+} correlated blood progenitor pairs (same pairs as in *B*). Each value $F_g(x)$ in the plot is the probability of a pair in group *g* to have a Pearson correlation coefficient greater than *x*. The Kruskal–Wallis statistical test verified a significant difference between the two distributions (*P*-value < 0.0001). See also *SI Appendix*, Fig. S1*B* for an analysis of all cell pairs. (*D*) Representative confocal images showing a Ca^{2+} signaling propagation event, detected by ARCOS, which defined a transient community involving six blood progenitors (*Results* and *Materials and Methods*). GCaMP6f is labeled in green. The center of each cell is marked in red (active, i.e., showing Ca^{2+} influx) or blue (inactive). Time (T, in second) is annotated in each frame. Orange polygons visualize the cell centers transiently participating in a community in each frame. White arrows indicate the inclusion of new activated cells in the community, yellow arrowheads indicate the deactivation and exclusion of cells from the community. All the cells that participate in the community throughout its evolution are marked in the last frame (T = 00:25) in a dashed white polygon. (Scale bar: 5 μm.) (*E*) Schematic of the spatial shuffling analysis (*Materials and Methods*). (1) Single-cell segmentation and extraction of Ca^{2+} time series. (2) Random spatial shuffling of the Ca^{2+} time series of all cells, repeated 1,000 times, correspondingly generating spatially permuted experiments. (3) ARCOS binarization: Ca^{2+} peak detection (red). (4) ARCOS community detection (red, white is GCaMP6f). Recording of the mean collective events per cell (MEC) and statistical comparison of MEC for observed versus in silico permuted experiments. (Scale bar: 5 μm.) (*F*) Analysis of MEC magnitude (N = 12 LGs). Ratio between MEC of the observed and the average MEC among its in silico permuted experiments. The ratio of value 1 (dashed horizontal line) implies no change in the magnitude. The bootstrapping significance test showed spatial significance for 11/12 LGs (color-filled circles). The one LG that was deemed insignificant had the fewest cells and transient communities making it more sensitive in terms of the MEC magnitude and the statistical significance. See *SI Appendix*, Fig. S5 for full analysis of all 12 LGs. (*G–I*) Gap junction inhibition experiments. Wild-type LGs (N = 12), RNAi-mediated *zpg* knockdown (N = 8), 3.125 μM CBX (N = 3), 12.5 μM CBX (N = 4), and CBX washout (N = 4). Statistical analyses: **P* < 0.05, ***P* < 0.01, ****P* < 0.001, *****P* < 0.0001. (*G*) Spatially significant experiments. For each experimental condition, gray indicates the number of insignificant and color indicates the number of significant LGs. Significance was determined using Fisher's exact test. (*H*) Analysis of MEC magnitude. Each data point corresponds to one LG. Significance was determined using the Kruskal–Wallis test to evaluate the differences between the wild-type and the other conditions. (*I*) Analysis of intercellular signaling propagation speed between adjacent cells in a community. Each data point (red) represents the average cell–cell signaling propagation speed calculated according to the relative activation timing between adjacent pairs in each transient community (*Materials and Methods*). Wild-type (N = 113 communities, mean information spread μ = 1.63 μm/s), RNAi-mediated *zpg* knockdown (N = 39, μ = 0.99 μm/s), 3.125 μM CBX (N = 62, μ = 1.35 μm/s), 12.5 μM CBX (N = 1, μ = 0 μm/s), and CBX washout (N = 71, μ = 1.41 μm/s). This analysis was performed to experiments that were imaged with temporal resolution of 2.32 to 4 s per frame (*Materials and Methods*), including 1/4 CBX 12.5 μM experiments (an experiment that did not exhibit communities, and therefore was not appropriate for statistical testing). Statistical significance was determined using the Kruskal–Wallis test to evaluate the differences between the wild-type and the other conditions.

treated with 100 μM CBX and then washed it out (N = 4). Analysis of these different treatment groups showed that gap-junction inhibition led to a drastic decrease in the fraction of experiments with significant local communities (Fig. 1*G*), the magnitude of collective signaling communities (Fig. 1*H*), and the intercellular signaling propagation speed between adjacent cells (termed intercellular signaling propagation speed, Fig. 1*I*). Intriguingly, washout experiments that were previously shown

to rescue the network properties and cell–cell propagation (9), partially rescued the magnitude of communities (Fig. 1*H*) and the intercellular signaling propagation speed between adjacent cells in a transient community (Fig. 1*I*), but did not rescue the fraction of collective signaling-event communities (Fig. 1*G*). These suggest that perturbation of gap junction-mediated communication may have a long-lasting effect on the signaling community that persists even after CBX is removed. The association between the LG's mean cell activation rate (i.e., frequency of cell activation), mean local cell density, and the MEC rate, meaning the mean frequency that a cell participates in a transient community, were maintained for most gap junction inhibition perturbations (*SI Appendix*, Fig. S7 *A-C*). However, Zpg depletion (using RNAi) or inhibition (using CBX) led to increased cell activation, i.e., higher frequency of Ca^{2+} spikes, but reduced MEC rate for the same activation level (*SI Appendix*, Fig. S7*D*), suggesting a compensation mechanism where Zpg-depleted or inhibited cells try to compensate for reduced cell–cell communication capacity by increasing their activity. These results validate the critical role of gap junctions in the formation of Ca^{2+}-based intercellular communities.

Recurrent Activation of Communication Communities Forms Hotspots of Local Information Processing Hubs. We next asked whether the same cells participate in multiple (transient) signaling communities, which, if true, could suggest that these communities act as signaling communication "hubs" that repeatedly receive and spread information to synchronize the multicellular network. To quantitatively assess this possibility in wild-type LGs, we recorded for each cell the number of times it participated in signaling communities. Visualization of the number of times each cell participated in a community revealed spatial heterogeneity with recurrent activation of specific communities, that we call "hotspots," involving groups of spatially adjacent cells with enriched participation in signaling communities with respect to the population (Fig. 2*A* and *SI Appendix*, Fig. S8 *A–D*; criteria used for hotspot identification are detailed in *Materials and Methods*). We identified hotspots that met these criteria in 9 out of the 12 wild-type (nontreated) LGs. The number of hotspots per LG ranged between 1 and 3 with each containing between 3 and 15 cells, with cells participating in a hotspot being more active than cells participating in communities, but not hotspots (*SI Appendix*, Fig. S9). To verify that hotspots were not a mere consequence of this increased cell activation we devised a bootstrapping-based statistical test (Fig. 2 *B–D*). First, we matched and replaced at least 50% of the cells in the hotspot with other cells in the same experiment that did not take part in the hotspot and had, at minimum, the same amount of activations. Second, we switched the Ca^{2+} time series for each pair of matched hotspot and nonhotspot cells, and then detected collective signaling events in this in silico, spatially permuted, experiment (Fig. 2*D*). Third, we recorded the MECs for cells participating in the hotspot of the in silico permuted experiment. We repeated these steps of switching "hotspot" with nonhotspot cells with at least the same number of Ca^{2+} activation, up to 1,000 times for each hotspot, recorded the difference between experimentally observed hotspots and their in silico permuted versions, and determined the statistical significance. Statistical significance was determined by calculating the fraction of permutations where the hotspot MEC values in the in silico experiments were equal to or exceeded the MEC values of the observed (wild-type, nonpermuted) experiment. This analysis showed a dramatic decrease in the MEC following spatial permutation (*SI Appendix*, Fig. S8 *E–L*), statistically validating 8 of 14 hotspots, spread over 5 of the 12 live intact ex vivo cultured LGs (Fig. 2*E*). The emergence of hotspots could not be explained by more Ca^{2+} activity or by higher pairwise within-community correlation in the Ca^{2+} signaling (*SI Appendix*, Fig. S10 *A* and *B*). Qualitative observation of the location of validated hotspots did not identify a specific spatial pattern of their distribution within the LG. Finally, we uncovered a role for gap junctions in the formation of maintenance of hotspots. Specifically, CBX-mediated perturbation of gap junctions, showed a reduction in the number of validated hotspots, and this effect persisted even after the CBX was removed by washout (Fig. 2*E*).

Our findings raised two important questions regarding the interaction of hotspots with their environment. First, do hotspots function as self-contained groups of cells, interacting predominantly within their enclosed local surroundings? Second, do hotspots initiate the spread of information, or are they more responsive to incoming nonhotspots external signals? Following the evolution of a transient community showed alternating interactions between cells inside and outside a hotspot (Fig. 2*F*). To systematically decipher the interactions between hotspots and their surrounding environment we analyzed the spatiotemporal communication patterns of all the validated hotspots that were pooled across the wild-type LGs (N = 8 hotspot). To quantify the interactions of hotspots with their surrounding cells, we calculated for each hotspot its probability of engaging with cells outside the hotspot through common transient communities (*Materials and Methods*). The majority of hotspots (7 out of 8) interacted with nonhotspot cells in more than half of their transient communities, this interaction was independent of the size of a hotspot (Fig. 2*G*), and was dominated by communities that involved two to four cells within the hotspot and one to two cells external to the hotspot (Fig. 2*H*). Specifically, 70% of hotspot communities had at least one nonhotspot cell involved, and 76% of these communities involved more hotspot cells than nonhotspot cells (Fig. 2*H*). These interactions of a hotspot with its surrounding cells did not have a systematic direction, starting from hotspot cells outward or initiating externally from adjacent nonhotspot cells (*SI Appendix*, Fig. S11; see *Materials and Methods*). Furthermore, we did not identify cells that repeatedly initiated a hotspot's transient communities, suggesting stochasticity in hotspot initiation. These observations established the existence of gap-junction-mediated communication hotspots, where recurrent Ca^{2+} communities coalesce into larger communication hubs that repeatedly spread and retrieve information throughout the blood progenitors.

Gradual Formation of Communication Communities and Their Recurrent Activation during LG Development. In flies, hematopoiesis is subject to developmental regulation, with blood progenitors exhibiting distinct behaviors at different larval stages (15, 16). Specifically, cell proliferation and differentiation show distinct patterns at different points along the developmental timeline (Fig. 3*A*) (16). For example, the differentiation of mature blood cells starts around the mid- to late-second instar transition and peaks around the mid-second to mid-third instar larval stages (10, 15, 16). The level of mature blood cell differentiation gradually declines as the LG develops and becomes significantly attenuated upon entry into the mid-third instar stage (Fig. 3*A*) (10, 16). In contrast, cell proliferation in the blood progenitors peaks earlier, during the first- to second-instar stages, when the progenitor repertoire rapidly expands (15, 16). Shortly after the onset of differentiation, the rate of cell proliferation slows down but remains active until the mid-third instar stage (Fig. 3*A*) (17).

We previously showed that Ca^{2+} signaling appeared to evolve over larval development, correlating with the differentiation activity of progenitors (9). Specifically, we observed lower Ca^{2+} signaling

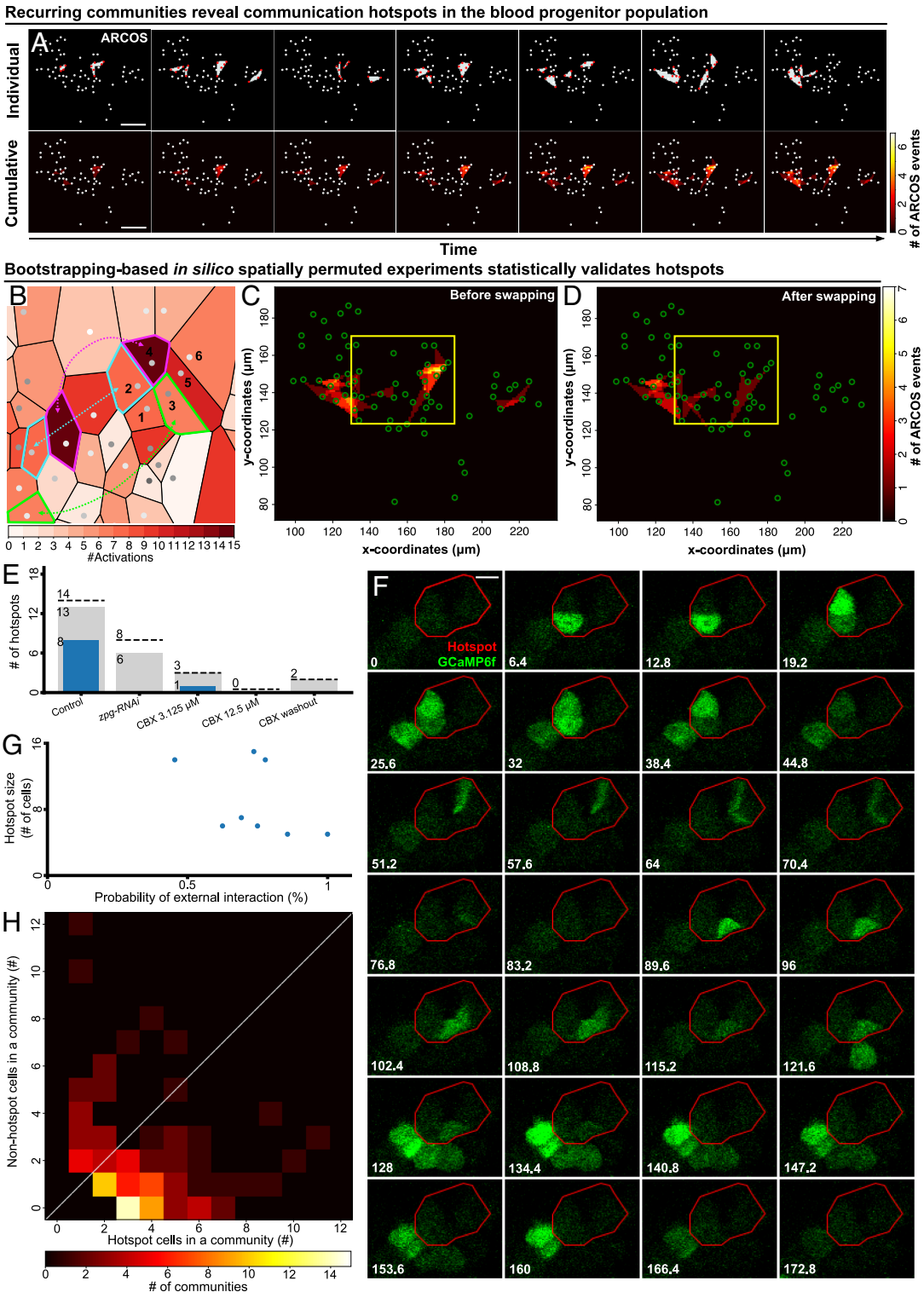

Fig. 2. Recurrent activation of communities forms hotspots that act as local information hubs. (*A*) Representative time-lapse images showing the formation of hotspots over time. A hotspot is defined by recurring transient communities (*Materials and Methods*). *Top* panels: transient communities (marked by colored polygons, red dots mark activated blood progenitors) in a wild-type LG. *Bottom* panels: the integrated number of transient communities over time. Each white dot represents an individual blood progenitor. Each panel corresponds to its matching *Top* panel. (Scale bar: 15 μm.) (*B*) Single-cell Voronoi tessellation, corresponding to the yellow region of interest shown in panels (*C*) and (*D*), and illustrating the bootstrapping-based in silico permutation experiment (*Materials and Methods*). The color of each cell (polygon) reflects the number of activations (i.e., Ca^{2+}spikes) each cell exhibits. Six cells that participate in a hotspot are numbered and dashed color-matched arrows indicate cell swapping. The swapping is performed for cell pairs with similar activation, where one cell is within and the other outside the hotspot (*Materials and Methods*). (*C* and *D*) Representative field of view showing the integrated number of transient communities each cell participated in over time (#ARCOS events) before (*C*) and after (*D*) in silico permutation [see (*B*)]. Green circles: the center location of each blood progenitor. Brighter areas indicate more occurrences of communities. The yellow region of interest marks the hotspot that is also shown in (*B*). (*E*) Hotspot statistics. Hotspots were pooled across experiments according to the experimental condition. Dashed line—pooled number of hotspots. Gray—pooled number of hotspots with sufficient data for statistical analysis. Blue—number of statistically significant validated hotspots. Hotspot significance was determined according to 100 to 1,000 different in silico permutation experiments with a bootstrapping significance threshold of 0.05. (*F*) Time-lapse evolution of a representative hotspot. The hotspot was defined according to the integrated number of transient communities per cell across the experiment (red polygon; see *Materials and Methods*). Transient communities involve cells within and outside the hotspot. GCaMP6f labeled in green. (Scale bar: 5 μm.) (*G*) The probability of hotspot cells interacting with cells outside the hotspot through common transient communities as a function of the hotspot's size (i.e., the number of cells in the hotspot). The analysis included the eight statistically verified hotspots pooled across all wild-type LGs. (*H*) Histogram of the number of hotspot cells (x-axis) and nonhotspot cells (y-axis) in communities that define the hotspots—each observation used for this histogram is defined by a community. White diagonal ($y = x$) indicates an equal proportion between hotspot to nonhotspot cells.

propagation between neighboring cells and a reduced connectivity of the Ca^{2+} signaling network during early larval stages (9). To understand how Ca^{2+} signaling communities develop during hematopoiesis when progenitors show distinct proliferation and differentiation patterns (Fig. 3*A*), we expanded our analysis to the earlier stages of the late-second and early-third larval stages. Our analysis characterized a gradual build-up of signaling communities, in terms of both quantity and complexity, over the course of blood progenitor development. Specifically, both the fraction of experiments with significant local communities (Fig. 3*B*) and the

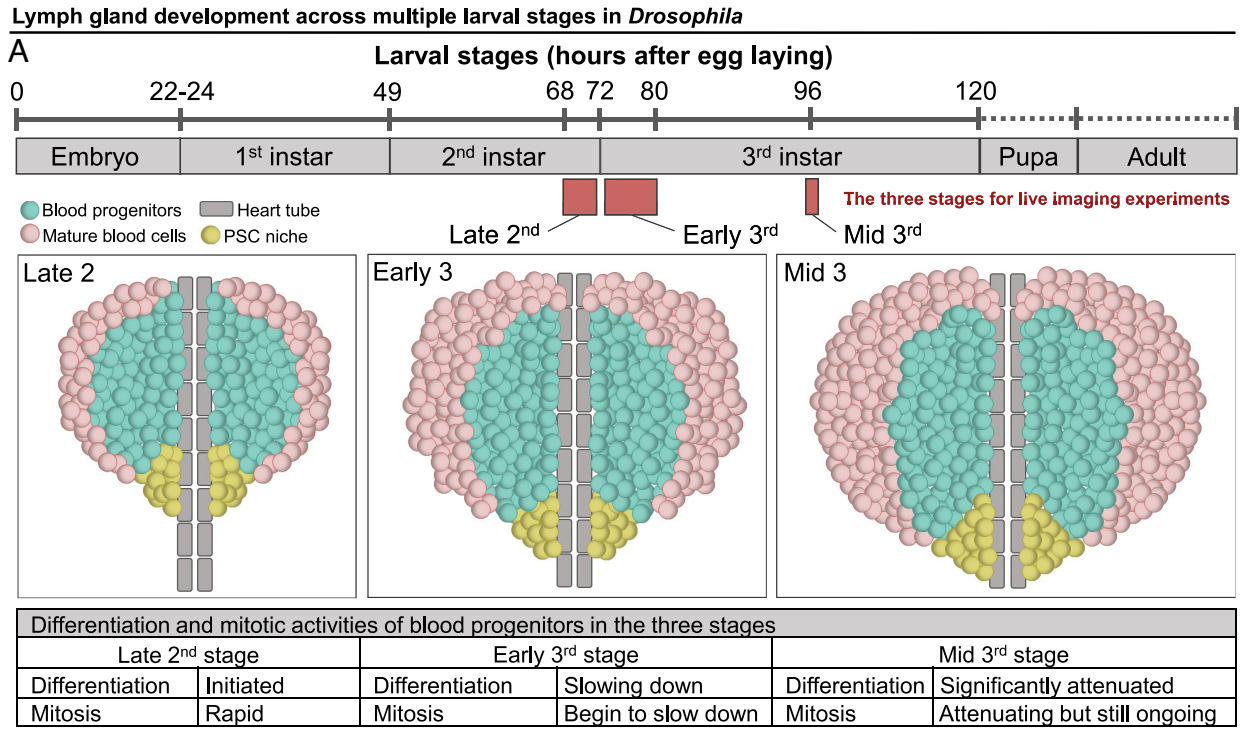

Differentiation and mitotic activities of blood progenitors in the three stages					
Late 2nd stage		Early 3rd stage		Mid 3rd stage	
Differentiation	Initiated	Differentiation	Slowing down	Differentiation	Significantly attenuated
Mitosis	Rapid	Mitosis	Begin to slow down	Mitosis	Attenuating but still ongoing

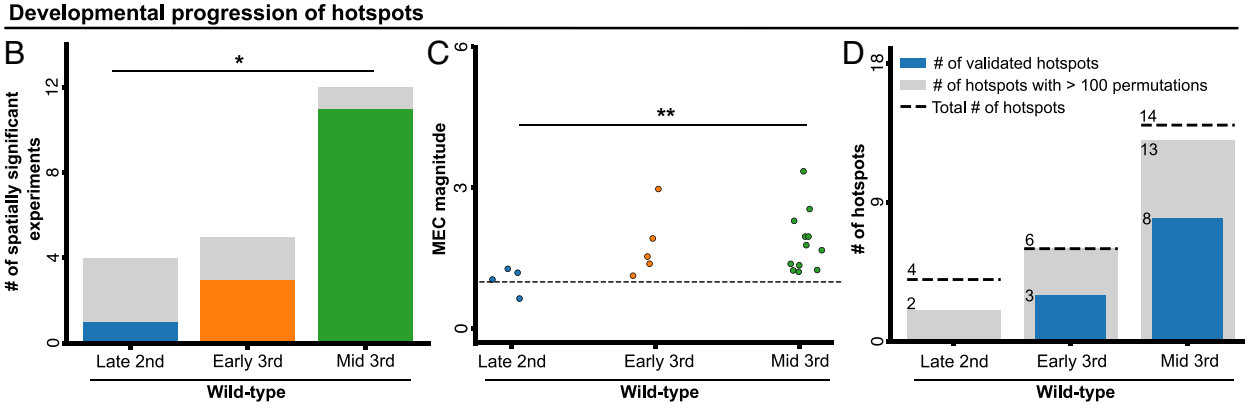

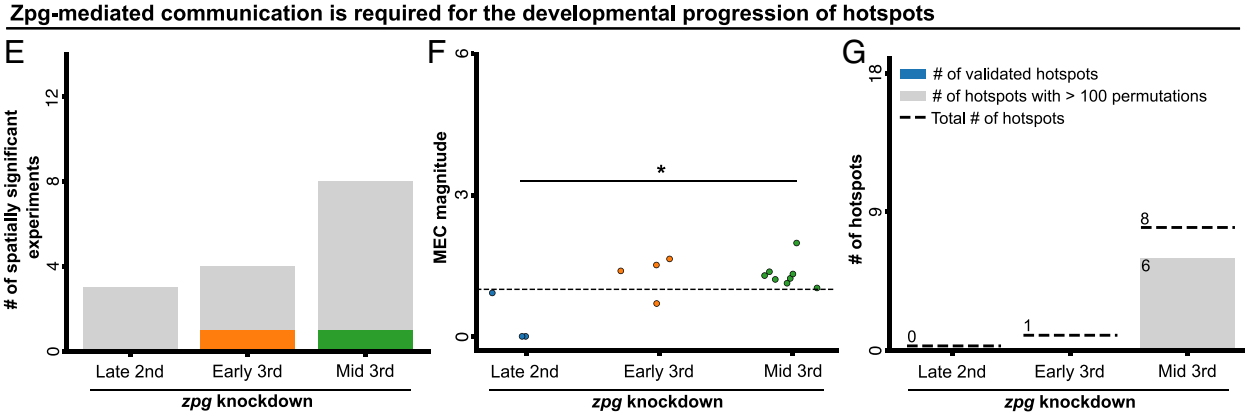

Fig. 3. Gradual formation of communication communities during development. (*A*) LG development throughout *Drosophila* larval stages (*Materials and Methods*). Differentiation and mitotic activities of blood progenitors across the three stages are summarized in the table. (*B–D*) Analyses of wild-type LGs from the late-second instar stage (N = 4), early-third instar stage (N = 5), and mid-third instar stage (N = 12). (*B*) Number of spatially significant experiments. For each experimental condition, gray indicates the number of insignificant and color indicates the number of significant LGs. Significance was determined using Fisher's exact test. (*C*) MEC magnitude. Each data point corresponds to a single LG. Significance was determined using the Kruskal–Wallis test to evaluate the differences between the different developmental stages. (*D*) Hotspots statistics. Dashed line—pooled number of hotspots. Gray—pooled number of hotspots with sufficient data for statistical analysis. Blue—number of statistically significant validated hotspots. Hotspot significance was determined according to 100 to 1,000 different in silico permutation experiments with a bootstrapping significance threshold of 0.05. (*E–G*) Analyses of RNAi-mediated *zpg* knockdown LGs from late-second instar stage (N = 3), early-third instar stage (N = 4), and mid-third instar stage (N = 8). (*E*) Quantification of the number of spatially significant experiments in blood progenitors. See (*B*). (*F*) Analysis of MEC magnitude. See (*C*). (*G*) Number of validated hotspots per developmental stage. See panel (*D*).

magnitude of MEC (Fig. 3*C*) increased across the three stages in wild-type LGs. In contrast, RNAi-mediated *zpg* knockdown induced a decrease in both parameters of signaling communities (Fig. 3 *E* and *F*), suggesting that the emergence of signaling communities was perturbed. Hotspots analysis showed a similar trend of gradual emergence of recurrent Ca^{2+} communities along the developmental trajectory with 0/4 statistically validated hotspots in the late-second, 3/6 in the early-third, and 8/14 in the mid-third stage (Fig. 3*D*). In contrast, no (0) hotspots were validated across all developmental stages of the Zpg-depleted LGs (Fig. 3*G*). Taken together, our data suggests that signaling communities and their recurrent activation (i.e., hotspots) emerge during, and evolve over, the course of larval development and that gap junctions are required for the developmental progression of these Ca^{2+} signaling communities in blood progenitors. This is also consistent with our previous observation showing that Zpg depletion increases blood cell differentiation (9), supporting a model where signaling communities coordinate blood progenitor behavior to maintain LG homeostasis during development.

Discussion

There are numerous examples in the literature reporting synchronization and collective events in the context of cell signaling and behavior (13, 18, 19). A critical question that has remained underexplored is how does global, tissue-scale synchronization emerge from local cell–cell communication? More specifically, what are the intermediary steps involved in reaching the final synchronization state? In an attempt to provide some insight into the answers to these questions, we have previously described how endothelial monolayers synchronize Ca^{2+} signaling by gradually transitioning from local to global information spread (19). Other studies reported signaling waves propagating across long distances in a variety of systems and in the context of diverse functions (13, 20–22). However, these studies did not pinpoint a specific intermediate spatial scale between single-cell and collective signaling. Here, using *Drosophila* hematopoiesis as our model system, we were able to identify such an intermediate spatial scale. Our work elaborates on our previous findings that described the important role played by gap junctions in coordinating cellular signals in the LG (9). In this earlier work, we demonstrated that stochastic and spontaneous Ca^{2+} waves propagate between progenitors and form a signaling network that transfers information across dispersed progenitor cells, and identified an important regulatory role of this network in coordinating collective cell fate decisions during hematopoiesis and development (9). However, the questions of how the signaling network is established progressively and how local cell–cell communication events become integrated over many cells to achieve tissue-level coordination remained unknown. We now revealed an intermediate spatial scale exists, involving transient gap junction-mediated Ca^{2+} signaling in the form of multicellular communities. Similar scale collective events were previously reported in the context of Erk signaling in epithelial cells, and Ca^{2+} signaling in the Madin-Darby canine kidney epithelium (13) suggesting that this could be a universal way to collectively organize the signaling activity of individual cells in a multicellular system.

A key feature in some of these transient communities was recurrent activation events that formed larger communication processing hubs that we call signaling hotspots. These hotspots had several important functional characteristics: 1) Their formation required the activity of Zpg-based gap junctions. 2) They acted as information hubs that were able to induce (i.e., transmit) and process (i.e., receive) collective signaling using mechanisms that operated both within (intrinsically) and outside (extrinsically) of the hotspot. 3) They exhibited repetitive interactions with their environment and were spatially heterogeneous. 4) There was an increased incidence of hotspots as the LG evolved and developed consistent with a role in the emergence of collective cell behavior. Each of these characteristics of the hotspots played an important functional role in shaping the signaling landscape within the LG. Overall, these findings reveal a mechanism whereby local cell–cell signaling propagation, through gap junctions, progresses into intermediate multicellular communities that integrate local information to achieve global population-wide synchronization during fly hematopoiesis.

Only 5 of the 12 LGs exhibited statistically significant hotspots, mainly due to the stringent statistical criteria we used for defining hotspots in order to avoid false positives (*Materials and Methods*). It is possible that our definition of hotspots falls along a more continuous spectrum of intercellular communication with different "magnitudes" of the communities' recurrence. From a physiological perspective, it is possible that not all LGs exhibit hotspots concurrently: Hotspots may appear transiently at key developmental transitions or in response to specific external cues. From a technical perspective, cross-LG variations in the numbers and spatial organization (e.g., density) of progenitor cells, variation in temporal imaging resolution and sensitivity of our Ca^{2+} reporter may limit our ability to identify hotspots. Overall, the combination of our rigorous statistical analysis, along with consistent results of gradual formation of hotspots during developmental stages in a gap-junction-dependent manner support our belief that Ca^{2+} signaling hotspots are a general phenomenon that occurs in LGs even if, due to technical limitations, it is not always straightforward to detect them in all instances.

Our observation that hotspots self-organize as information processing hubs in the blood progenitor population suggests that the hotspots perform a function that bears general resemblance to that performed by pacemaker cells, at the multicellular scale. A characteristic of pacemaker cells is their ability to coordinate the electrical or Ca^{2+} signaling activity of individual cells to guide collective decisions (18, 23, 24). Multicellular structures that are functionally and morphologically similar to pacemaker cells appear across diverse tissues, including Cajal interstitial cells in the gut (25), a sinoatrial node in the heart (24), and preBötC cells in the brainstem (26), indicating that it is a conserved module in living systems to regulate systemic homeostasis. We note three features of blood progenitor hotspots that resemble those found in pacemaking cells. First, as we previously proposed, blood progenitors form a small-world Ca^{2+} signaling network (9), where most cells are separated from each other by a small number of cell-to-cell transmission events thanks to a small subgroup of cells with high connectivity compared to other cells (12). Here, using ARCOS and in silico spatial permutation analysis, we directly demonstrated the existence of such hub-like network structures, or hotspots, within the blood progenitor population. Second, a well-known feature of pacemaker cells is their ability to integrate and segregate information between cells that are either external or internal to their signaling hub (27–29). Our study quantitatively illustrates that Ca^{2+} signaling in blood progenitors is organized into hotspots that are able to both receive and send information. Third, there are several functional analogies between the hotspots found in blood progenitors and cardiac pacemaker cells found in sinoatrial nodes. These include: A) transfer of information across large distances and the ability to fine-tune the activities of a large group of cells (24), B) highly synchronized multicellular activity that is often tied to function (9, 24, 30), C) coordinated cell behavior that is dependent on gap junctions

(9, 30), D) self-organization and synchronization of local heterogeneous Ca^{2+} signals (24), and E) intracellular Ca^{2+} signals in both systems are controlled by the same molecular machinery including gap junctions (9, 23, 30), SERCA pumps (9, 31), and ryanodine receptors (10, 31). These observations highlight similar design principles, both conceptual and functional, that allow LG blood progenitor hotspots and cardiac pacemaker cells to coordinate cells within a population.

Signaling hotspots highlight the spatial heterogeneity in intercellular Ca^{2+} information processing in the developing LG. How such heterogeneity develops in seemingly homogenous blood progenitors remains unknown. One possible mechanism is through heterogeneity in intercellular communication that can arise from intrinsic cell-to-cell variation in gene expression levels or protein modifications (32–34). Indeed, single-cell transcriptomic analysis on LGs showed that blood progenitors, which were previously considered as a homogenous population, exhibited a large variability in their gene expression profiles (35–38). This variability allowed the classification of progenitors into six main subclusters that showed distinct spatial distribution and gene expression profiles (35). Such differences in gene expression could contribute to the heterogeneity of Ca^{2+} signaling. Additionally, the position of the progenitors within the LG could impact their ability to receive signals that control progenitor function (39). For example, both the PSC and differentiated blood cells produce cues that control blood progenitor function (7, 37, 40). We previously demonstrated that the movement and distribution of signaling molecules within the LG is controlled by septate junctions as well as by the ECM (41). In particular, we observed that components of the ECM including Collagen, Laminin, and Nidogen, assemble into a fibrous network that separates proximal blood progenitors into small clusters and regulates the movement of signaling molecules through the extracellular space (41). This patchy topology could, in theory, generate the heterogeneity that underlies Ca^{2+} signaling hotspots. Links between ECM distribution and hotspots should be explored in the future. Finally, another possible mechanism underlying the emergence of hotspots is their clonal origin. Exploring this option is possible by visualizing clonal labeling along with Ca^{2+} dynamics but is technically challenging.

The identification of Ca^{2+} signaling hotspots in the LGs raises the question of their possible physiological role. Since Ca^{2+} signaling regulates several major downstream signaling pathways and consequently blood cell differentiation (9, 40), two possible roles for hotspots are regulating downstream blood progenitor signaling or modulating progenitor differentiation. Previous studies, including our own work (9), have analyzed spatial heterogeneity in various developmental signaling pathways that function in blood progenitors including the activity and distribution of the JAK-STAT, CaMKII, Wnt/Wingless, and Dpp/BMP pathways (9). However, looking back at our published data, we were unable to see obvious spatiotemporal patterns of these signals that matched with the characteristics of hotspots (9). In contrast to cell signaling, we were able to identify spatiotemporal differences in the LG in cell differentiation. Specifically, we recently reported an analysis of spatiotemporal patterns of differentiation in live LGs that revealed spatial heterogeneity in the distribution of differentiation events, with differentiation "clusters" in distinct regions in the LG (15). Based on these observations we propose that it is theoretically possible that there is a connection between hotspots and differentiation clusters. However, determining whether this is indeed the case would require a complex experimental setup and further investigation.

The emergence of hotspots from oscillating blood progenitors required a mechanism that coordinates their individual activities. Although we demonstrated that the function of Zpg-based gap junctions was indispensable in this process, the underlying mechanism remains unclear. We can envision several possible routes for the emergence of collective Ca^{2+} signaling hotspots in the blood progenitor population. According to theoretical, physics, and neural-based studies, routes giving rise to collective behaviors can be classified into four main categories (42): A) Pacemaker cells, in this context cells that fire rhythmic signals, entraining other cells to oscillate or behave in a synchronized fashion (43). B) Phase and/or frequency locking, where cells that naturally oscillate at different frequencies synchronize their behaviors by adjusting their phases and/or frequencies when coupled with other cells, a representative example being circadian neurons (44–47). C) Oscillator death, where mathematical approaches and synthetic genetic clocks show that cells stop oscillating when coupled with other cells (42, 48). Therefore, decreasing the coupling strength permits the emergence of synchronized behavior. D) Dynamic quorum sensing, where nonoscillatory cells start oscillating when a signaling molecule they secrete exceeds a critical concentration threshold in their environment, an example being yeast glycolytic oscillations (42). Comparing our data with the above four categories, we proposed that hotspot emergence likely involves a hybrid mechanism with both pacemaker-like and phase/frequency locking properties. First, we noticed that some progenitors were still able to produce Ca^{2+} spikes even in the presence of a high concentration of CBX (9), indicating that these cells spontaneously produce spikes without the need of neighbor connections. As discussed in the previous section (Hotspots act as information hubs), the progenitor hotspots show characteristics consistent with having pacemaker-like properties. Second, for the phase/frequency locking property, we found that the complexity and incidence rate of hotspots increased concomitant with animal development. This showed that hotspots are able to accommodate or incorporate new cells in a developing progenitor population. Our previous observations show that the number of gap junctions increased, and the spiking frequency of blood progenitors was modulated during LG development (9). These two lines of evidence suggest that the newly incorporated cells, once coupled with other cells, changed their spiking frequency over time, consistent with the phase/frequency locking phenomenon. Overall, we suggested that the progenitor hotspots emerge by simultaneously utilizing the pacemaker-like and phase/frequency docking mechanisms. Taken together, our findings align with other recent studies that reported collective signaling in the spatial scale of multiple cells (13, 49, 50), suggesting a universal mechanism to collectively organize the signaling activity of individual cells in a multicellular system.

Materials and Methods

***Drosophila* Genetics, Stocks, and Maintenance.** All *Drosophila* stocks and crosses were maintained regularly on a standard cornmeal medium (recipe from the Bloomington *Drosophila* Stock Center) in vials or bottles at 25 °C. The blood progenitor-specific Gal4 driver used was *Tep4-Gal4* (a kind gift from Lucas Waltzer, Université Clermont Auvergne, France). Other lines used were *UAS-GCaMP6f* (RRID:BDSC_42747) and *UAS-zpg-RNAi* (RRID:BDSC_35607). Larvae were staged as follows: Eggs were first collected 6 to 8 h after egg laying (AEL), late-second instar larvae were collected 68 to 72 h AEL, early-third instar larvae were collected 72 to 80 h AEL, and mid-third instar larvae (or wandering third instar larvae) were collected 96 h AEL (9).

Sample Preparation and Confocal Imaging. To prepare live LG samples, larvae in desired stages were washed using Phosphate-Buffered Saline (PBS) three times (2 min each), quickly rinsed with 70% ethanol, washed again with PBS three times (2 min each), and dissected in the *Drosophila* Schneider's medium (prewarmed to room temperature 10 min prior dissection; ThermoFisher

Scientific, 21720001). The dissected LG was mounted in the glass bottom dishes (MatTek Corporation, 35 mm, P35G-0-14-C, noncoated), covered with a 1% agar pad (Agar A, Bio Basic, FB0010, prepared in the Schneider's medium), and stabilized with 1% agar spacers to prevent LG compression during live recordings (15). The dish was supplied with 2 mL Schneider's medium over the agar pad for moisture and placed in a microscope incubator (TOKAI HIT, Catalog number: INU-ONICS F1) that maintains the temperature at 25 °C during imaging. LG optical sections spaced by 1.5 μm were imaged using a 40× oil immersion objective (numerical aperture 1.30, UPLFLN) on an Olympus inverted confocal microscope (FV1000) with a temporal resolution ranging from 2.3 to 6.7 s per frame (9).

To monitor real-time Ca^{2+} signals in blood progenitors, a genetically encoded Ca^{2+} sensor GCaMP6f (peak excitation ~480 nm, peak emission ~510 nm) was expressed. Fiji (51) was used to manually annotate circular ROIs around each progenitor cell according to the GCaMP6f activity. Raw GCaMP6f intensity values were extracted at the ROIs at individual time points (z-profile Fiji plugin) and exported to Excel (in .csv format). The obtained GCaMP6f signals of each cell were normalized, $F'_t = (F_t - F_{min})/(F_{max} - F_{min})$ where F_t = raw GCaMP6f value at each time point, F_{min} and F_{max} = minimum and maximum GCaMP6f values of a cell, respectively) (9, 15). Time-lapse recordings were processed in Fiji and Fluoview (Olympus FV10-ASW 4.2) and the data were analyzed using Python. No stabilization or registration on images was performed. Intensities represented mean gray values.

To block gap junctions, live dissected LGs were incubated in 50 or 100 μM CBX (Sigma, CG4790) for 15 min, mounted in the Schneider's medium with corresponding CBX concentration, and imaged immediately (9). For the CBX-washout experiment, LGs were incubated in 100 μM CBX for 15 min, rinsed in the Schneider's medium twice (5 min each), mounted, and imaged immediately (9). A 1 mM CBX stock was stored at −20 °C. Imaging settings were set identically across experiments.

Transient Communities Detection and Analysis. We applied ARCOS (13) to detect and quantify the Ca^{2+} collective signaling events in blood progenitors. We applied the ARCOS Python implementation (arcos4py, version 0.1.5) on the normalized time series for each inspected LG. We set the parameter *neighborhoodSize*, the distance threshold for synchronous activation, to 14 μm, which represents about two cell diameters (*SI Appendix*, Fig. S2 *A* and *B*). *minTotalEventSize* was set to three cells, and indicates the overall number of cells participating throughout the evolution of a transient collective signaling event. *minClsz* was set to 1 cell, and indicates the minimum number of cells simultaneously activated at each time frame throughout the evolution of a transient collective signaling event. These settings enable the detection of transient communities forming via gradual sequential intercellular signal propagation even in communities that involve a single activated cell at each time frame. *nPrev*, the maximal number of time frames between different cell activations, was configured empirically to a maximum time lag of 15 s. *minDuration*, the minimal time for a collective event to occur, was set to 1 frame, enabling the detection of short-term co-occurring activations. Binarization parameters were set according to the default recommended values (13), with *biasMet*, *smoothK* and *biasK* set to "runmed," 3 and 25, respectively. To minimize the detection of false activations, peakThr and binThr were empirically set to 0.3 and 0.4, respectively.

Relative Ca^{2+} Spikes Magnitude. Ca^{2+} spikes for each cell were determined according to the ARCOS analysis (13). For each cell we calculated the mean and SD of its "background" Ca^{2+} signal in all inactive frames, defined as all frames at least 3 frames before or after a Ca^{2+} spike. Next, we measured the relative Ca^{2+} spike magnitude as the z-score in respect to each cell's background Ca^{2+} signal. Finally, the relative Ca^{2+} spike magnitude of a cell was defined as the mean z-score of its spikes.

Statistically Validating Local Properties of Collective Signaling Events. We designed a bootstrapping-based statistical test to reject the null hypothesis that the collective signaling events are nonlocal properties. This was achieved by repeating the following steps 1,000 times: A) spatially shuffling the cells' time series, which is equivalent to randomizing the cells' locations; B) applying ARCOS to the spatially shuffled time series; C) recording the mean number of collective signaling events per cell (mean events per cell, MEC) across the spatially shuffled cells. The statistical significance was calculated as the fraction of spatially shuffled experiments where the MEC was equal to or exceeded the MEC of the observed (not shuffled) experiment, with "spatial significance" set at 0.05. The MEC magnitude was calculated as the ratio between the experimentally observed MEC and the mean MEC of all of its spatially shuffled experiments, and indicates the MEC fold change in respect to excluding the spatial organization. The following formula exemplifies the magnitude calculation for experiment exp and its N spatial permutations denoted by $\overline{\exp_i}$:

$$\text{Magnitude}_{\exp} = \text{MEC}_{\exp} / \frac{\sum_i^N \text{MEC}_{\overline{\exp_i}}}{N}.$$

Mean Local Cell Density and Mean Cell Activation. The mean local cell density was defined as the average number of cells within a square area of 14 × 14 μm^2 surrounding each cell. The mean activation rate was defined as the average number of activations per cell per minute. Both measurements were calculated according to the mean value of all cells in each LG.

Communities' Intercellular Signaling Propagation Speed. The intercellular signaling propagation speed of a community was defined as the mean time difference between the activation of adjacent cells as a function of the distance between these cells (μm/s) in the context of the transient community. This community-specific measurement was pooled across all LGs within each experimental condition. To avoid confounding effects due to different temporal resolutions between experiments, we excluded experiments that had temporal resolution outside the range of 2.32 to 4 s per frame, leaving the following number of LGs per experimental condition: $N_{\text{wild type late 2nd}} = 4$; $N_{\text{wild type early 3rd}} = 5$; $N_{\text{wild type mid 3rd}} = 4$; $N_{\text{zpg RNAi late 2nd}} = 3$; $N_{\text{zpg RNAi early 3rd}} = 3$; $N_{\text{zpg RNAi mid 3rd}} = 3$; $N_{\text{CBX 3.125}} = 2$; $N_{\text{CBX 12.5}} = 1$, $N_{\text{CBX washout}} = 4$.

Hotspots Analysis. We defined LG_{max} as the maximal number of transient communities in which a single cell participated within a specific LG. We calculated an LG-specific threshold: $LG_{threshold} = \max\left(5, \frac{LG_{max}}{2}\right)$, and marked all cells that participated in at least $LG_{threshold}$ transient communities. For each connected component (in the neighborhood graph) group of adjacent cells above this threshold we calculated its convex hull and considered it as a hotspot candidate. To validate that a hotspot was not a result of random effects nor physical confounding factors (*Materials and Methods*: Mean local cell density and mean cell activation), we conducted a bootstrapping-based statistical test as follows. First, we matched at least 50% of the hotspot cells with other nonhotspot cells from the same LG, where each of the nonhotspot cells had at least the same number of Ca^{2+} activation as its matching hotspot cell. Second, we swapped the Ca^{2+} time series of each matched pair of hotspot and nonhotspot cells. Third, we employed ARCOS on the in silico spatially permuted LG to detect collective signaling events. Fourth, we recorded the MEC for the permuted hotspot cells. Fifth, we repeated these four steps for each hotspot up to 1,000 times, hotspot candidates with at least 100 different in silico spatially permuted LGs were considered for the bootstrapping-based significance test. For each hotspot candidate, the statistical significance was determined as the percentage of in silico permutations that yielded equal or greater MEC values compared to the original nonpermuted LG. A hotspot candidate with a P-value ≤ 0.05 was considered as a validated hotspot.

Interactions between Hotspots and Their Surrounding Environment. We quantified the interaction between cells within hotspots and their adjacent nonhotspot cells, and measured the temporal ordering of the cells' activation. Hotspot community was each transient community that included at least one hotspot cell. For each hotspot, we calculated the ratio between the number of hotspot communities involving both hotspot and nonhotspot cells to the total number of hotspot communities (also including hotspot-exclusive cells). This ratio represents the probability of hotspot cells interacting, via a transient community, with nonhotspot cells.

The direction of interaction between hotspot and nonhotspot cells was defined as whether a hotspot community was initiated by a hotspot or a nonhotspot cell. This analysis focused on hotspot communities involving at least one nonhotspot cell. We defined two measurements for directionality: A) The fraction of hotspot communities that were initiated by hotspot cells. For this measurement, we excluded hotspot communities that were initiated by both hotspot and nonhotspot cells that appeared in the same time frame, because of the ambiguity to which cell initiated the community. B) For each hotspot transient community, we considered all cell pairs comprising one hotspot cell and one nonhotspot cell, within a distance ≤14 μm from one another. We calculated the transmission

probability as the fraction of such pairs where the hotspot cell was activated before the nonhotspot cell.

The hotspot size was defined as the number of cells participating in the hotspot. The proportion of hotspot cells in transient communities was defined as the fraction of hotspot cells in a community. This proportion was averaged across all hotspot communities to define the average proportion of hotspot cells in transient communities, which was used as the expected probability of a hotspot cell to be the initiator of a hotspot transient community, under the assumption of random activation order of cells within a community.

Statistical Analysis. Pearson correlation (scipy.stats.pearsonr) was used to measure the correlation between the Ca^{2+} signals of blood progenitors (Fig. 1 *B* and *C* and *SI Appendix*, Figs. S1 *A* and *B* and S6), the correlation between MEC rate, mean local cell density, and mean cell activation rate (*SI Appendix*, Figs. S4 and S7), and the correlation between hotspot size and its activation rate (*SI Appendix*, Fig. S10*A*). Bootstrapping was applied in the spatial shuffle analysis (e.g., Fig. 1*E*) and the hotspot shuffle analysis (e.g., Fig. 2*C*). Fisher's exact test (scipy.stats.fisher_exact) was used to measure the differences between different experimental conditions (treatments) in terms of the amount of spatially significant LGs (e.g., Figs. 1 *F* and *G* and 3 *B* and *E*). Fisher's exact test was chosen due to the small sample size in each experimental condition, and due to the categorical nature of the data. The Kruskal–Wallis test (scipy.stats.kruskal) was used to measure the difference between the distributions of cell pair Pearson correlation of Ca^{2+} signals (Fig. 1*C* and *SI Appendix*, Figs. S1*B*, S6, and S10*B*), magnitude of Ca^{2+} spikes (*SI Appendix*, Fig. S3), magnitude of MEC (Figs. 1*H* and 3 *C* and *F* and *SI Appendix*, Fig. S5), community-level information spread rate (Fig. 1*I*), activation rate (*SI Appendix*, Fig. S9), and distance distribution comparison (*SI Appendix*, Fig. S7*D*) across experimental conditions. The nonparametric Kruskal–Wallis test was chosen due to the varying sample sizes across different experimental conditions and due to the unknown underlying distribution of our data. All significance tests were carried out with an α-value of 0.05, considering $^{*}P < 0.05$, $^{**}P < 0.01$, $^{***}P < 0.001$, $^{****}P < 0.0001$.

Data, Materials, and Software Availability. Further information and requests for resources and reagents should be directed to and will be fulfilled by the lead contacts: Assaf Zaritsky (assafzar@gmail.com) and Guy Tanentzapf (guy.tanentzapf@ubc.ca). All materials and reagents used in this study are documented in *Materials and Methods*. All the source codes and sample data developed in this study are publicly available from the Zaritsky Laboratory GitHub (https://github.com/zaritskylab/recurring-transient-communities) (52). All other data are included in the manuscript and/or supporting information.

ACKNOWLEDGMENTS. We acknowledge the Bloomington *Drosophila* Stock Center. We thank Dr. Lucas Waltzer for providing fly stocks. Research at the Zaritsky laboratory is supported by the Israel Council for Higher Education (CHE) via the Data Science Research Center, Ben-Gurion University of the Negev, Israel, by the Israel Science Foundation (ISF, grantNo. 2516/21), by the Israel Ministry of Science and Technology (MOST), by the Wellcome Leap Delta Tissue program, by the German-Israeli Foundation (GIF)-Nexus, and by the Rosetrees Trust. Research in the lab of G.T. is supported by the Canadian Institutes of Health Research (Project Grant PJT-156277). K.Y.L.H. is supported by a Four-Year Doctoral Fellowship from the University of British Columbia. We thank Dr. Bo Sun, Dr. Dagan Segal, and Dr. Julia Mack for critically reading the manuscript.

1. F. Julicher, S. Eaton, Emergence of tissue shape changes from collective cell behaviours. *Semin. Cell Dev. Biol.* **67**, 103–112 (2017).
2. R. Mayor, S. Etienne-Manneville, The front and rear of collective cell migration. *Nat. Rev. Mol. Cell Biol.* **17**, 97–109 (2016).
3. B. L. Bassler, How bacteria talk to each other: Regulation of gene expression by quorum sensing. *Curr. Opin. Microbiol.* **2**, 582–587 (1999).
4. M. G. Surette, M. B. Miller, B. L. Bassler, Quorum sensing in Escherichia coli, Salmonella typhimurium, and Vibrio harveyi: A new family of genes responsible for autoinducer production. *Proc. Natl. Acad. Sci. U.S.A.* **96**, 1639–1644 (1999).
5. L. Capuana, A. Bostrom, S. Etienne-Manneville, Multicellular scale front-to-rear polarity in collective migration. *Curr. Opin. Cell Biol.* **62**, 114–122 (2020).
6. S. Toda, N. W. Frankel, W. A. Lim, Engineering cell-cell communication networks: Programming multicellular behaviors. *Curr. Opin. Chem. Biol.* **52**, 31–38 (2019).
7. U. Banerjee, J. R. Girard, L. M. Goins, C. M. Spratford, Drosophila as a genetic model for hematopoiesis. *Genetics* **211**, 367–417 (2019).
8. C. J. Evans, T. Liu, J. R. Girard, U. Banerjee, Injury-induced inflammatory signaling and hematopoiesis in Drosophila. *Proc. Natl. Acad. Sci. U.S.A.* **119**, e2119109119 (2022).
9. K. Y. L. Ho, R. J. Khadilkar, R. L. Carr, G. Tanentzapf, A gap-junction-mediated, calcium-signaling network controls blood progenitor fate decisions in hematopoiesis. *Curr. Biol. CB* **31**, 4697–4712. e4696 (2021).
10. J. Shim *et al.*, Olfactory control of blood progenitor maintenance. *Cell* **155**, 1141–1153 (2013).
11. J. Mathews, M. Levin, Gap junctional signaling in pattern regulation: Physiological network connectivity instructs growth and form. *Dev. Neurobiol.* **77**, 643–673 (2017).
12. E. Smedler, S. Malmersjo, P. Uhlen, Network analysis of time-lapse microscopy recordings. *Front. Neural Circuits* **8**, 111 (2014).
13. P. A. Gagliardi *et al.*, Automatic detection of spatio-temporal signaling patterns in cell collectives. *J. Cell Biol.* **222**, e202207048 (2023).
14. R. Bauer *et al.*, Intercellular communication: The Drosophila innexin multiprotein family of gap junction proteins. *Chem. Biol.* **12**, 515–526 (2005).
15. K. Y. L. Ho, R. L. Carr, A. D. Dvoskin, G. Tanentzapf, Kinetics of blood cell differentiation during hematopoiesis revealed by quantitative long-term live imaging. *eLife* **12**, e84085 (2023).
16. J. Krzemien, J. Oyallon, M. Crozatier, A. Vincent, Hematopoietic progenitors and hemocyte lineages in the Drosophila lymph gland. *Dev. Biol.* **346**, 310–319 (2010).
17. B. C. Mondal *et al.*, Interaction between differentiating cell- and niche-derived signals in hematopoietic progenitor maintenance. *Cell* **147**, 1589–1600 (2011).
18. B. Sun, J. Lembong, V. Normand, M. Rogers, H. A. Stone, Spatial-temporal dynamics of collective chemosensing. *Proc. Natl. Acad. Sci. U.S.A.* **109**, 7753–7758 (2012).
19. A. Zamir *et al.*, Emergence of synchronized multicellular mechanosensing from spatiotemporal integration of heterogeneous single-cell information transfer. *Cell Syst.* **13**, 711–723.e717 (2022).
20. K. Aoki *et al.*, Propagating wave of ERK activation orients collective cell migration. *Dev. Cell* **43**, 305–317.e305 (2017).
21. N. Hino *et al.*, ERK-mediated mechanochemical waves direct collective cell polarization. *Dev. Cell* **53**, 646–660.e648 (2020).
22. P. A. Gagliardi *et al.*, Collective ERK/Akt activity waves orchestrate epithelial homeostasis by driving apoptosis-induced survival. *Dev. Cell* **56**, 1712–1726.e1716 (2021).
23. K. T. Moortgat, T. H. Bullock, T. J. Sejnowski, Gap junction effects on precision and frequency of a model pacemaker network. *J. Neurophysiol.* **83**, 984–997 (2000).
24. R. Bychkov *et al.*, Synchronized cardiac impulses emerge from heterogeneous local calcium signals within and among cells of pacemaker tissue. *JACC. Clin. Electrophysiol.* **6**, 907–931 (2020).
25. M. Y. Lee *et al.*, Transcriptome of interstitial cells of Cajal reveals unique and selective gene signatures. *PloS one* **12**, e0176031 (2017).
26. J. L. Feldman, K. Kam, Facing the challenge of mammalian neural microcircuits: Taking a few breaths may help. *J. Physiol.* **593**, 3–23 (2015).
27. N. Takahashi, T. Sasaki, W. Matsumoto, N. Matsuki, Y. Ikegaya, Circuit topology for synchronizing neurons in spontaneously active networks. *Proc. Natl. Acad. Sci. U.S.A.* **107**, 10244–10249 (2010).
28. M. Rubinov, O. Sporns, Complex network measures of brain connectivity: Uses and interpretations. *NeuroImage* **52**, 1059–1069 (2010).
29. A. L. Barabasi, Z. N. Oltvai, Network biology: Understanding the cell's functional organization. *Nat. Rev. Genet.* **5**, 101–113 (2004).
30. M. R. Boyett, H. Honjo, I. Kodama, The sinoatrial node, a heterogeneous pacemaker structure. *Cardiovascular Res.* **47**, 658–687 (2000).
31. H. Musa *et al.*, Heterogeneous expression of Ca(2+) handling proteins in rabbit sinoatrial node. *J. Histochem. Cytochem. Official J. Histochem. Soc.* **50**, 311–324 (2002).
32. M. B. Elowitz, A. J. Levine, E. D. Siggia, P. S. Swain, Stochastic gene expression in a single cell. *Science* **297**, 1183–1186 (2002).
33. G. Gut, M. D. Herrmann, L. Pelkmans, Multiplexed protein maps link subcellular organization to cellular states. *Science* **361**, eaar7042 (2018).
34. A. Raj, A. van Oudenaarden, Nature, nurture, or chance: Stochastic gene expression and its consequences. *Cell* **135**, 216–226 (2008).
35. B. Cho *et al.*, Single-cell transcriptome maps of myeloid blood cell lineages in Drosophila. *Nat. Commun.* **11**, 4483 (2020).
36. N. S. Dey, P. Ramesh, M. Chugh, S. Mandal, L. Mandal, Dpp dependent Hematopoietic stem cells give rise to Hh dependent blood progenitors in larval lymph gland of Drosophila. *eLife* **5**, e18295 (2016).
37. R. Baldeosingh, H. Gao, X. Wu, N. Fossett, Hedgehog signaling from the posterior signaling center maintains U-shaped expression and a prohemocyte population in Drosophila. *Dev. Biol.* **441**, 132–145 (2018).
38. J. R. Girard *et al.*, Paths and pathways that generate cell-type heterogeneity and developmental progression in hematopoiesis. *eLife* **10**, e67516 (2021).
39. B. Hudry *et al.*, Sex differences in intestinal carbohydrate metabolism promote food intake and sperm maturation. *Cell* **178**, 901–918.e916 (2019).
40. K. Y. L. Ho *et al.*, Maintenance of hematopoietic stem cell niche homeostasis requires gap junction-mediated calcium signaling. *Proc. Natl. Acad. Sci. U.S.A.* **120**, e2303018120 (2023).
41. R. J. Khadilkar, K. Y. L. Ho, B. Venkatesh, G. Tanentzapf, Integrins modulate extracellular matrix organization to control cell signaling during hematopoiesis. *Curr. Biol. CB* **30**, 3316–3329.e3315 (2020).
42. P. Mehta, T. Gregor, Approaching the molecular origins of collective dynamics in oscillating cell populations. *Curr. Opin. Genet. Dev.* **20**, 574–580 (2010).
43. P. S. Chen *et al.*, The initiation of the heart beat. *Circul. J. Off. J. Japanese Circul. Soc.* **74**, 221–225 (2010).
44. C. Liu, D. R. Weaver, S. H. Strogatz, S. M. Reppert, Cellular construction of a circadian clock: Period determination in the suprachiasmatic nuclei. *Cell* **91**, 855–860 (1997).
45. A. G. Siapas, E. V. Lubenov, M. A. Wilson, Prefrontal phase locking to hippocampal theta oscillations. *Neuron* **46**, 141–151 (2005).
46. T. L. To, M. A. Henson, E. D. Herzog, F. J. Doyle IIIrd, A molecular model for intercellular synchronization in the mammalian circadian clock. *Biophys. J.* **92**, 3792–3803 (2007).
47. E. Ullner, J. Buceta, A. Diez-Noguera, J. Garcia-Ojalvo, Noise-induced coherence in multicellular circadian clocks. *Biophys. J.* **96**, 3573–3581 (2009).

48. E. Ullner, A. Zaikin, E. I. Volkov, J. Garcia-Ojalvo, Multistability and clustering in a population of synthetic genetic oscillators via phase-repulsive cell-to-cell communication. *Phys. Rev. Lett.* **99**, 148103 (2007).
49. L. Valon *et al.*, Robustness of epithelial sealing is an emerging property of local ERK feedback driven by cell elimination. *Dev. Cell* **56**, 1700–1711.e1708 (2021).
50. K. W. Pond *et al.*, Live-cell imaging in human colonic monolayers reveals ERK waves limit the stem cell compartment to maintain epithelial homeostasis. *eLife* **11**, e78837 (2022).
51. J. Schindelin *et al.*, Fiji: An open-source platform for biological-image analysis. *Nat. Methods* **9**, 676–682 (2012).
52. S. B. David, K. Y. L. Ho, G. Tanentzapf, A. Zaritsky, Formation of recurring transient Ca^{2+}-based intercellular communities during *Drosophila* hematopoiesis. GitHub. https://github.com/zaritskylab/recurring-transient-communities/tree/main/data. Deposited 11 March 2024.